1-1-1994

Late-time behavior of stellar collapse and explosions. II. Nonlinear evolution

Carsten Gundlach
The University of Utah

Richard H. Price
The University of Utah

Jorge Pullin
The University of Utah

Recommended Citation

Gundlach, C., Price, R., & Pullin, J. (1994). Late-time behavior of stellar collapse and explosions. II. Nonlinear evolution. *Physical Review D, 49* (2), 890-899. https://doi.org/10.1103/PhysRevD.49.890

NSF-ITP-93-85
gr-qc/9307010

Late-time behavior of stellar collapse and explosions: II. Nonlinear evolution

Carsten Gundlach, Richard H. Price and Jorge Pullin

Department of Physics, University of Utah, Salt Lake City, UT 84112-1195

(9 July, 1993)

Abstract

We compare the predictions of linearized theory for the radiation produced in the collapse of a spherically symmetric scalar field with a full numerical integration of the Einstein equations. We find power-law tails and quasinormal ringing remarkably similar to predictions of linearized theory even in cases where nonlinearities are crucial. We also show that power-law tails develop even when the collapsing scalar field fails to produce a black hole.

I. INTRODUCTION

Linearized perturbation theory has been the main analytical – and until comparatively recently, numerical – tool for analyzing nonspherical gravitational collapse. The complexity of the problem has usually made this approach necessary, and it has been assumed until recently that the approach was sufficient. Recently, however, Gómez and Winicour [1] have focused attention on the extent to which these results are even qualitatively representative of the late stages of collapse.

In the picture given by linear perturbation theory of the late stages of collapse, there are two features which are noteworthy. One is the development of "quasinormal (QN) oscillations," damped oscillations at complex frequencies characteristic of the mass of the black hole background. The second feature is the decay in time t of perturbations as $1/t^n$, the "power-law tails." There are good reasons to examine more carefully whether these features also appear in the fully nonlinear case. The arguments for the QN oscillations and for the tails are somewhat different, and should be considered separately.

According to linearized theory the QN frequencies are fixed complex numbers multiplied by the inverse of the mass of the black hole background. (We use here and throughout units in which $c = G = 1$.) It seems reasonable that the phenomenon of QN ringing will be a feature of nonlinear collapse. One argument is that some numerical investigations of solutions of the fully nonlinear equations have shown QN ringing to be common [2]. Secondly, the idea of QN ringing seems "robust." It is a natural frequency associated with a radiative boundary condition, and can occur in many different radiative systems. If QN ringing is found, to what black hole mass does it correspond? The QN oscillations themselves carry energy and may change the meaning of the mass. A reasonable guess, at least, can be made that the QN frequency evolves somewhat during the collapse.

The situation for the power-law tails is quite different. These tails are not familiar or common phenomena. The explanation of their existence can be given in two very different ways: (i) They can be viewed as the result of the scattering of gravitational waves off the

"effective curvature potential" of the black hole spacetime [3], or (ii) they can be associated with the branch cut in the Green function for the wave propagation problem [4]. Both arguments leave open the possibility that the tails are idiosyncrasies of the linear approximation.

If QN oscillations or tails are missing from a fully nonlinear collapse, or if there is any significant new qualitative feature, the result might be to undermine confidence in the picture of collapse given to us by the analysis of linear perturbations of black hole backgrounds. Gómez and Winicour [1] have addressed this question with numerical studies of the collapse of a spherically symmetric scalar field due to its own gravitational pull. Since the spherically symmetric problem involves only a 1+1 hyperbolic system, it is enormously easier to solve numerically than the problem of nonspherical collapse.

What is more, the problem is a wonderful testing ground for comparing nonlinear results and the predictions of linearized theory. In linearized perturbation theory the evolution of a scalar field is governed by essentially the same mathematics that governs the dynamics of nonspherical perturbations. In particular, perturbation theory makes very specific predictions about QN ringing and tails for perturbative spherically symmetric scalar fields. It is therefore of great interest that in their initial numerical studies of scalar field collapse, Gómez and Winicour have seen neither QN ringing nor tails.

In this paper we will study the fully nonlinear evolution of a scalar field minimally coupled to general relativity. We consider first the evolution of a spherically collapsing scalar field; in addition, we consider nonspherical perturbations of this spacetime. We establish that the QN frequencies and the power-law tails of the numerical simulations are in remarkable agreement with the predictions of linearized theory when a black hole develops. If a black hole does not develop, and all energy eventually radiates away to infinity, we find that power-law tails still form. The existence of tails, but not QN oscillations, when holes do not form agrees with the analysis presented in the companion paper, hereafter referred to as Paper I.

The organization of this paper is as follows. In section II we describe the coordinate system and the version of the field equations we use. In section III we describe our discretization and discuss the numerical error. In section IV we study the collapse of a scalar field for var-

ious initial configurations. In section V we study the evolution of multipole moments of test fields on the collapsing background. In all cases comparisons with the linearized results are made. We end in section VI with a brief summary and with conclusions.

II. FIELD EQUATIONS AND ALGORITHM

We study a spherically symmetric scalar field ϕ satisfying the minimally coupled equation

$$\phi^{;\mu}_{\ ;\mu} = 0. \tag{1}$$

To describe the spherically symmetric spacetime we use the line element [5,6],

$$ds^2 \equiv -g(u,r)\bar{g}(u,r)\,du^2 - 2g(u,r)\,du\,dr - r^2\,d\Omega^2, \tag{2}$$

in which u is a retarded time null coordinate. Regularity at the center requires that $g = \bar{g}$ at $r = 0$. The remaining coordinate freedom is fixed by the choice that u be the proper time on the $r = 0$ central world line, or $g = \bar{g} = 1$ at $r = 0$. We introduce the auxiliary field ψ by

$$\phi \equiv \frac{1}{r}\int_0^r \psi\,dr. \tag{3}$$

In terms of this variable, the wave equation (1) for ϕ takes the form

$$\left(\frac{\partial}{\partial u} - \frac{\bar{g}}{2}\frac{\partial}{\partial r}\right)\psi \equiv D\psi = \frac{1}{2r}(g-\bar{g})(\psi-\phi). \tag{4}$$

The metric coefficients g and $\bar{g}$ are determined from ϕ by

$$g = \exp\left[4\pi\int_0^r \left(\frac{\partial\phi}{\partial r}\right)^2 r\,dr\right], \tag{5}$$

$$\bar{g} = \frac{1}{r}\int_0^r g\,dr. \tag{6}$$

Because of the spherical symmetry there is no independent gravitational degree of freedom. The operator D in (4) differentiates along ingoing null characteristics, and information is propagated along outgoing null characteristics (the u = constant lines) by (3). The

integration scheme of equations (3) and (4) can therefore be related to a fully characteristic coordinate system ($u =$"retarded time", $v =$"advanced time,") in which the metric takes the form

$$ds^2 = -f(u,v)\,du\,dv + r^2(u,v)\,d\Omega^2, \tag{7}$$

and in which $D \propto \partial/\partial v|_u$. Here the coordinate v is fixed only up to arbitrary transformations $v \to \tilde{v}(v)$. Since the coordinate is only a label on the ingoing null geodesics it can be assigned values $v = 1, 2, 3...$ on our numerical grid.

Our algorithm works on a characteristic grid made up of lines of constant u and v, with the radial "coordinate" r treated as a metric function $r(u,v)$ which is evolved as

$$D\,r = -\bar{g}/2\ . \tag{8}$$

As initial data for the algorithm we take $\psi(v)$ and $r(v)$ on an initial outgoing null cone $u = u_0$. These are equivalent to the choice of null data $\phi(r)$ and the (arbitrary) numerical choice of the initial position in r of each ingoing null lines of the grid (i.e., each line of constant v). The algorithm, which closely resembles that of Goldwirth and Piran [6], proceeds as follows: We start by using (3) to obtain ϕ and by using (5) and (6) to obtain g and $\bar{g}$ as functions of v along $u = u_0$. (The integrations over r are discretized as summations over v.) We next choose a value of the "time step" Δu, and we use (4) to obtain ψ, and (8) to obtain r, at grid points along $u = u_0 + \Delta u$. The process is then repeated starting with the new outgoing characteristic $u = u_0 + \Delta u$. On each such cycle of integrations the step size Δu is chosen so that

$$|r(v, u + \Delta u) - r(v,u)| \leq |r(v+1, u) - r(v,u)| \tag{9}$$

for all $v = 1, 2, 3, ...$ This has been found to be a useful rule of thumb. Since our integration scheme proceeds along characteristics, there can be no violation of causality, and hence there is no formal "Courant condition" to satisfy.

Figure 1 shows our uv grid embedded in the well-known conformal diagram of spherical collapse. Null lines $u = const.$ and $v = const.$ are at 45 degrees. Infinity has been brought

to a finite distance and each point, apart from the line $r = 0$, corresponds to a 2-sphere of surface $4\pi r^2$. This diagram shows where our null data are set and how far they are evolved. The upper left and right sides of our coordinate patch, though at finite distances, can be taken as approximations of the horizon $\mathcal{H}_+$ and future null infinity $scri_+$. Lines of constant r go from past to future timelike infinity. Those with $r < 2M_f$, where M_f is the final mass of the black hole, cross the event horizon, while $r = 2M_f$ approaches it asymptotically. This gives one numerical method for finding the final black hole mass. Another is to take the limit of the Bondi mass $M_B(u)$ at late retarded times $u \to \infty$, where

$$M_B(u) \equiv \lim_{r\to\infty} \left(1 - \frac{\bar{g}(u,r)}{g(u,r)}\right) r^2 \,. \tag{10}$$

Yet another spacetime coordinate will be useful in comparing our results to analytic predictions, although it plays no active role in our algorithm. This additional coordinate is defined as the proper time along an $r = const.$ trajectory, or

$$t = t(u,r) \equiv \int_0^u \sqrt{g(u',r)\bar{g}(u',r)}\, du'. \tag{11}$$

We shall also use Bondi time, $t_B \equiv t(u,\infty)$, which is the retarded time coordinate that agrees with time at infinity for constant r. In an asymptotically flat spacetime the large r limit of $t(r)$ is given by $dt_B = \lim_{r\to\infty} \bar{g}(r,u)\, du$.

Our code has limited integration time precisely because it is characteristic. By definition u is the proper time of an observer at $r = 0$. The event horizon starts spreading out from $r = 0$ at a finite value of u, say u_h. In a collapse $\bar{g}(\infty,u)$ becomes infinite as $u \to u_h$. In our algorithm this means that the stepsize Δu decreases rapidly, while Δt_B remains about constant. The numerical approach to the horizon is stopped eventually by an overflow of $\bar{g}$ or underflow of Δu. The situation is best illustrated in Fig. 2. The $u = const.$ lines of our grid are squeezed together against the horizon. The problem of over/underflow, and of numerical instability (which usually develops earlier) is shared by all codes which avoid singularities by staying outside apparent horizons. A possible cure would be a slicing which does cross the horizon, combined with simply discarding parts of each slice inside the horizon. If the

surface beyond which time slices are discarded eats into the remaining part of the grid with the speed of light or faster, no boundary condition is required on it [7]. Such a procedure is not applicable to a characteristic grid, where the "time" slice is already an outgoing null cone and cannot be intersected by one.

III. DISCRETIZATION AND ERROR ANALYSIS

As we have just seen, our grid is highly nonuniform in u if a horizon forms. In that case it becomes also highly nonuniform in r. Ingoing null geodesics pile up at $r = 2M_f$, even if v is chosen uniform in r on the original slice. Truncation error is reduced, of course, if the grid spacing is made finer. We have tried to produce a code that is second-order accurate under a uniform grid rescaling. We denote here the relative size of the grid spacing by h; a reduction by a factor 2 of h means that the spacing in r is reduced by 2 and, due to the Courant-like condition (9), the spacing Δu is also reduced by 2.

On the top level we treat each of equations (4) and (8) as an ordinary differential equation in u at each fixed v. These are solved by the second-order Runge-Kutta method. The calculation of the "coefficients" ϕ, r, g and $\bar{g}$ in these "ODEs" is nontrivial however, and couples the equations at different values of v. They are given by the definite integrals (3), (5) and (6), which must be evaluated in that order. The integrals are discretized by the trapezoidal rule, which is again formally second-order accurate.

In principle our code should be second-order. That is, for the finite difference approach we use, the error at a given spacetime point should vary as h^2. We did not find this second-order convergence one would expect naively from the code, but did find convergence better than first order. One reason for the failure of a simple error analysis is the ambiguity about the measure of error. As the dynamical range of ϕ and the other fields is very large in a collapse spacetime, there is little point in taking an l_2, l_1 or l_∞ norm of the error in the fields over a set of spacetime points covering all of the integration region. The regions where the fields are large would dominate the integrated error. What is relevant to our confidence in

the results is the *relative* error, in particular in the regions where we are looking for tails and where ϕ is small.

Because of this we have looked at small spacetime regions, taking the l_2 norm over only a few neighboring points. For all these regions we found power-law dependence of errors to apply over a change in grid size by a factor of 16. Roughly speaking, error scaled as h^N, with $N = 1$ for small r or small t_B, and increasing up to 1.6 for both r and t_B large. By small r we mean the very narrow shell in r, just outside $r = 2M_f$, in which ϕ remains large at all times and where its gradient increases without bound. By small t_B we mean the region where the bulk of outgoing radiation passes.

Figures 3 and 4 display the error in of $\phi(r, t_B)$, for sections of the lines $r = 10$ and $t_B = 50$. In these figures the initial data is a Gaussian $\phi(r, t_B = 0)$ with center 1.0, width 0.1 and amplitude 0.06. (See the next section for a general discussion of initial data.) As there are no useful analytical solutions available, we had to use a numerical solution as the reference solution. We chose a solution generated with an initial grid spacing of $\Delta r = 1/320$, and compared to it grid spacings of 1/20, 1/40, 1/60, 1/80, 1/120, 1/160 and 1/200. (In all of these, however, the grid spacing was smoothly reduced by another factor of 16 for grid values of $0 < r < 1$, as we shall explain below.) The values of ϕ for the lower-resolution runs were interpolated linearly to the values of r and t_B of the grid points of the highest-resolution run. The difference of ϕ between a run and the reference run was squared, summed and the square root taken.

Figures 5 and 6 establish visually that the code converges, by showing sections of $\phi(r = 10, t_B)$ for different grid spacing. Figure 5 shows the region dominated by QN ringing, and Fig. 6 a region dominated by the power-law tail.

It is perhaps surprising that the error varies as h^N, even if N varies over spacetime and does not have the value 2 that one might suppose. The fact, however, that this power is closer to 1 both near the origin and in regions of large ϕ, and closer to 2 elsewhere, seems to be an indication that the error is largely due to our handling of the $r = 0$ boundary conditions.

We were alerted by reference [8] to the possibility that the main source of error may be the boundary conditions $\bar{g} = g$ and $\phi = \psi$ at $r = 0$. It can be seen in Fig. 1 that one after another, the $v = const.$ grid lines cross $r = 0$ into unphysical negative values of r, at which point they are dropped from the algorithm. We have numerically implemented the $r = 0$ boundary condition by approximating the true value of $\psi(u, r = 0)$ by linear interpolation. Formally this is only first-order accurate. The situation is more involved, however: the right-hand side of (4) contains an explicit factor of $1/r$, which in the exact solution is cancelled by the very boundary condition we are trying to impose, and which analytically leads to $g - \bar{g} = O(r)$ and $\psi - \phi = O(r)$. The risk of large numerical error, or even numerical instability, is clear. Empirically we found that our linear approximation algorithm is stable, but gives rise to large errors at small u, which actually decrease with increasing u. We believe the reason is that at small u the scalar field ϕ is still large at $r = 0$, thus introducing a large error into the boundary condition. At large u, the field strength resides mostly at large r, and in this regime the standard discretization error is dominant. We addressed this problem, not by using higher-order interpolation, but by brute force. We made the grid much denser in r, typically by a factor of 16, up to and slightly beyond the radial scale of the initial data. This meant that the grid size was much smaller until the bulk of the energy in the scalar field had reached $r = 0$ and then had propagated out to large r. In this way we achieved a reasonably small relative error everywhere, small enough to give us confidence in our results.

In summary, our code is not second-order accurate, but better than first-order accurate. We achieved high enough accuracy to have a small relative error everywhere, but even at a much lower resolution the physical features we had set out to verify, QN ringing and power-law tails, are unambiguously present.

IV. SPHERICAL COLLAPSE

In this section we present our results for the purely spherical collapse of a self-gravitating minimally coupled scalar field. Our expectations are based on linearized perturbations as analyzed in the Paper I. Because the scalar field at late times has small amplitude, it seems plausible that the late-time fields can be viewed, roughly, as perturbations, and that the analysis of Paper I applies, at least approximately. Our expectations then include the presence of QN oscillations at late times after a black hole has formed, and power-law tails at late times, both when a black hole forms and when it does not. The real and imaginary part of the QN frequencies – the least damped mode is the only one visible in practice – are fixed numbers divided by the black hole mass. The powers of the linear theory tail are fixed integers. When there is a static scalar field present on the initial null slice, the amplitude of the power-law tail, in the linearized case, is also determined. The analysis in Paper I suggests that these predictions for a scalar test field should hold also, approximatively, if the spherically symmetric scalar field evolves under the influence of its own gravitational pull rather than on a fixed Schwarzschild background.

We examined two one-parameter families of initial data. In the first family the field is a Gaussian in r; we consider the Gaussian to represent a typical collapsing "shell of matter." There is a scale invariance in the problem which can be used to set the center of the Gaussian at $r = 1$; the remaining physical parameters are the Gaussian width and amplitude. A black hole will form from these initial data if the amplitude is sufficiently large, or if the Gaussian width is sufficiently small.

As a second family of data, two different forms of $\phi(u = 0, r)$ are joined. For r less than some joining radius $r_{\rm J}$, the solution is constant at $\phi = \phi_0$, and for $r > r_{\rm J}$, the initial data is taken to be that static solution of (1) which is well behaved as $r \to \infty$ (i.e., the solution which falls of as r^{-1}). This solution is called "static-static" [1] because it gives rise to a static spacetime in the domain of dependence of either the inner ($r < r_{\rm J}$) or outer ($r > r_{\rm J}$) initial data. Without loss of generality we can set the joining point at $r_J = 1$. The only free

parameter is then A, the field amplitude at that point. Again this one-parameter family should contain spacetimes with and without an event horizon.

Static-static data are the boundary between generic "shell" initial data and data which are not asymptotically flat. We found that when we replaced the exact static solution (given analytically as an implicit function in [9,1]) by $\phi = const./r$) the resulting solution is qualitatively different: it corresponds to an infall of matter at arbitrarily late times.

A first check of our code is the amplitude of static-static data at which a black hole first forms. We find $0.28 < \phi_0 < 0.29$, which agrees with the critical value $\phi_0 = 0.286$ given in [1]. For the Gaussian data we find $0.033 < A < 0.034$, where A is the height of the Gaussian. These limits are stable under reduction of the grid size by a factor of 16, from 1/20 down to 1/320, as described in the previous section.

A crucial feature of both Gaussian and static static data is that the amplitude (the value of ϕ_0 or the Gaussian height A) can be chosen either "subcritical" (no hole formation) or "supercritical" (a hole forms). By varying the amplitudes we found three different regimes for the resulting spacetimes. a) For the amplitude much greater than its critical value we found QN oscillations and tails qualitatively and, for the most part quantitatively, as predicted by linearized analysis. b) For the amplitude near its critical value we found the same power-law tails, but we found QN ringing to be qualitatively different in the Gaussian and static-static cases. c) For the amplitude smaller than its critical value (even marginally) we found the same power-law tails as for collapse, but no QN ringing.

We now discuss in more detail the results for power-law tails and for QN ringing, starting with the former. The analysis in Paper I shows that for linear spherical perturbations tails should fall off in time (time for a distant observer, or Bondi time) as t_B^{-3} in the case of generic data, and as t_B^{-2} for data corresponding to an initially static monopole moment. Figure 7 shows log-log plots of ϕ at a constant values of the radius (here $r = 10$) as a function of Bondi time for different values of the amplitude of the initial Gaussian data. At late times ϕ clearly decays as a power of Bondi time, t_B^{-n}. The measured exponents are in reasonably good agreement with the prediction of linearized theory: $n = 2$ for static static data, and $n = 3$ for

Gaussian data. These power-law tails develop, and have the same exponents, whether or not a hole forms, and the amplitude of the tails is a smooth function of the initial amplitude. For the development of a tail, hole formation is irrelevant. This independence of hole formation is explained by the argument in Paper I that tail development is due to backscatter at large r, and does not depend on the small r nature of the spacetime.

In the case of static-static data, the linear perturbation analysis of Paper I predicts not only the exponent of the tail, but the amplitude. If our static static data were evolving on a fixed Schwarzschild background of mass M, the Paper I prediction would be that at late times and large radii (specifically $t \gg r \gg M$) the tail would have the form $\phi = -4M\phi_0/t^2$. It is unclear just how to apply this in general to the time dependent spacetimes of our present numerical investigations. Since the mass of the spacetime is evolving, and might fall to zero, what value of "M" should be used in the prediction for the amplitude of the tail? The picture of scattering underlying the calculations of Paper I would suggest that the correct M is some average, over retarded time, of the mass. The question of the appropriate mass is not crucial in one subset of cases: collapse models in which the initial data leads to the formation of a hole of mass not very different from the initial Bondi mass. In this case one might expect the linear fixed background prediction to apply. Our results, however, do not show this. In all cases, whether subcritical or supercritical, the amplitude of the tail is an order of magnitude less than the prediction of linearized theory (using the initial Bondi mass for M in the above expression). The reason for this is not yet clear.

The results for QN ringing differ in an important way from those for tails. QN ringing is a late time oscillation associated with the "effective potential" governing the dynamics of perturbation fields outside a hole. Unlike the power-law tails, QN ringing depends on the small r nature of the spacetime. If a hole (or relativistically compact object) does not form, the generation of QN oscillations is not expected. This is verified by the results; we have found no QN ringing for solutions without black holes. The transition from solutions with QN ringing to solutions without is, however, qualitatively different for Gaussian and static-static data.

For Gaussian data, this transition is abrupt; QN ringing is clearly present in a marginally collapsing spacetime, and clearly absent in a marginally noncollapsing spacetime. This is strikingly illustrated in Fig. 8, showing the solutions evolved from Gaussian data with amplitudes 0.033 and 0.034. We plot ϕ as a function of Bondi time at constant radius. Initially the two solutions are close, as one would expect from the closeness of their initial data. Later, the collapsing solution is delayed with respect to the noncollapsing one, and shows QN ringing. But after QN ringing has died away, and the power law tail dominates both solutions, they are again close. This result is compatible with the linearized analysis given in Paper I. Power-law tails are the result of backscatter, at large r, of the initial outgoing burst of waves. The two near-critical curves in Fig. 8 have almost identical outgoing bursts (since they correspond to very nearly the same initial data) so, at late times, the tails should be the same. The QN ringing, on the other hand, depends on how the solution develops at small r and hence is expected to be very different for the subcritical and supercritical cases.

For static-static data, the QN ringing fades away gradually before the critical amplitude is reached from above. In consequence, $\phi(r = 10, t_B)$ is nearly the same function everywhere for marginally collapsing and noncollapsing data; see Figs. 9 and 10. It may be that the QN ringing is masked, in the marginally collapsing case, by the non-QN fields, but the explanation at present is not clear.

It is difficult to measure the QN frequencies for the spherical scalar field, as only one minimum and one maximum is visible. For an initial Gaussian of amplitude 0.06 for example, one measures a half-period of about 4.0. In this case the initial Bondi mass is 0.1699 and the final Bondi mass still 0.1696, so that the mass is practically constant. The half-period predicted for spherical scalar perturbations [10] is $28.44M$, so on the basis of linear perturbation theory we would expect a half period between 4.832 and 4.824, which agrees with what is seen in the numerical results within the rather unsatisfactory precision available.

V. PERTURBATIONS OF SPHERICAL COLLAPSE

To understand better the results of the nonlinear evolution of the spherically symmetric scalar field, we have investigated a closely related problem. We consider a second minimally coupled scalar field φ, not coupled to the ϕ field, and we treat this second field perturbatively. That is, we ignore the contribution of φ to the stress-energy, and hence to the spacetime geometry. We study, then, the evolution of the perturbative φ field on the backgrounds generated by collapsing ϕ fields. Since these backgrounds are spherically symmetric, the perturbations can be decomposed into spherical harmonics which decouple. The equations of motion for a perturbation of fixed angular dependence $\varphi = \varphi_l^m(u,r)Y_l^m(\theta,\phi)$ are simply

$$D\psi_l^m = \frac{1}{2r}(g-\bar{g})(\psi_l^m - \varphi_l^m) + \frac{1}{2r}l(l+1)g\varphi_l^m, \tag{12}$$

$$\varphi_l^m \equiv \frac{1}{r}\int_0^r \psi_l^m \, dr, \tag{13}$$

where g and $\bar{g}$ are still determined by the background solutions for ϕ, through (5) and (6). The last term in (12) turns out to drive instabilities near $r = 0$ for $l \neq 0$. The simple expedient of reducing the step size Δu to a value much smaller (we used 1/16) than that of condition (9) was found to remove the instability. (We are grateful to Jeffrey Winicour for suggesting this remedy.)

It should be understood that the equations governing φ are not quite the same as those that would describe perturbations of the ϕ field itself. The stress-energy tensor is quadratic in ϕ, so that a perturbation $\delta\phi$ in ϕ would give rise to a perturbation in the stress-energy tensor that is first order in $\delta\phi$, and proportional to the "background" value of ϕ. It follows that there would be a first order perturbation in the spacetime geometry. The equations governing $\delta\phi$ would therefore *not* be the equations for a minimally coupled field on the background spacetime given by the background ϕ solution. (The situation is similar to that for electromagnetic perturbations of the Reissner-Nordström spacetime. Since there is a background electromagnetic field, the equations for electromagnetic perturbations are

not simply the Maxwell equations on the Reissner-Nordström spacetime.) Despite this, one should expect that there is not a great deal of difference in the *late time* behavior of φ and of $\delta\phi$. Since the background ϕ field becomes very small at late times, the stress-energy perturbations should be very small.

The motivation for studying the φ field is that the scalar collapse models go beyond the models of Paper I in two distinct ways. First, the scalar collapses involve nonlinear field evolution, and second, they produce time dependent spacetime geometries on which the tails and the QN oscillations are developing. The introduction of a perturbation field allows us to separate these two complications. The dynamics of φ is purely linear, but takes place on the time dependent background spacetime. A study of the φ field has an additional attraction: For fixed backgrounds the exponents of the power-law tails depend on the multipole index l. For generic data the tails fall off as $t^{-(2l+3)}$; for initially static multipoles they fall off as $t^{-(2l+2)}$. By computing different multipoles of φ we can check whether this l dependence applies also to time dependent backgrounds. A further technical advantage is that multipole modes of higher l have QN frequencies which are considerably less damped than the least damped $l = 0$ mode. This allows us much more readily to "observe" the presence of QN oscillations and to measure their frequencies.

As an example we turn again to the solution with Gaussian data of amplitude 0.06, an example we considered in the previous section. For the φ test field we choose a Gaussian of width 0.1, the same width as for the background ϕ field, but we put the center of the φ Gaussian at 2.0 while the center of the ϕ Gaussian, which generates the background, is at 1.0. This means that the perturbation "shell" goes in later than the background shell, giving the black hole time to form. For the $l = 0$ φ field we again (as in section IV) find a half-period of about 4.0, and again find it difficult to determine the period with any accuracy, so that a meaningful comparison cannot be made with the fixed background prediction of 4.824 (calculated from a final Bondi mass of 0.1696). For the $l = 1$ φ field, however, we could see 10 oscillations, and could measure a half-period of 1.811, which is within 0.7 % of the predicted value of 1.819. For $l = 2$ there are 20 oscillations, with the measured half-period

of 1.105, within 0.2 % of the predicted value of 1.104. QN ringing for these cases is shown in Fig. 11.

We also examined $l = 2$ QN ringing on a background with considerable mass loss during the time of QN excitation. To arrange this a Gaussian "shell" of ϕ and a Gaussian "shell" of test field φ were both centered at $r = 1.0$. The ϕ field was chosen to have amplitude 0.033. This gives an initial Bondi mass of 0.05822 which decreases to a final Bondi mass of 0.02035, with most of the mass loss taking place during $2 < t_B < 4$. For these masses, linearized theory predicts that the frequency of the least damped $l = 2$ mode should go up from 8.31 to 23.87. This is in excellent agreement with our numerical results, within the inevitable uncertainty in measuring a varying frequency.

For power-law tails the most interesting backgrounds are those that are the most time dependent, the noncollapsing backgrounds. For these backgrounds results are shown in Fig. 12 for tails from Gaussian data with an amplitude of 0.020 and in Fig. 13 for tails from static-static data with an amplitude of 0.10. As these figures show, the late time behavior is rather accurately that of a power-law tail; the numerically determined exponents are in rough agreement with the predictions of linearized theory, and show the predicted increase of slope with multipole index l.

VI. DISCUSSION

In Paper I we revisited the argument [3] for the existence of power-law tails of perturbations of Schwarzschild spacetime, in order to point out that it predicts these tails not only at timelike infinity, but also at null infinity and on the horizon. Reformulating the argument yielded an important spin-off prediction: Power-law tails should form in general not only in perturbations of black holes. The analysis suggested that the tails should form for massless perturbations of any approximately spherically symmetric spacetime whose metric is approximately Schwarzschild, at least on an outgoing null cone of finite thickness (i.e., finite range of advanced time).

The central idea, as elaborated in Paper I, is quite simple. Radiation going out along a thick null cone (the "initial burst" of radiation) will be scattered back in by the spacetime curvature at arbitrarily large radius. The backscattered radiation then reaches a small radius again at arbitrarily large time, attenuated by a power of Bondi time. This backscattered radiation then evolves tails. The leading effect in this evolution is independent of spacetime curvature. The exponent of the tails is therefore the same if at late times there is, at small r, a star, empty space, or a black hole.

In our numerical work described here we first set out to verify the existence of the tails, as well as of QN ringing, in a collapse situation. We chose the model of a spherically symmetric self-gravitating massless minimally coupled scalar field, because tails and QN oscillations seemed to be absent in the results of a previous investigation [1]. The explanation of that absence seems to be simply that one has to go to very late times to see the late-time features. We did find tails and QN ringing precisely as expected. Fortunately these features arise about an order of magnitude in time before our code is stopped by a diverging redshift.

Extending the scope of previous work, we paid attention to the late-time behavior of solutions which are subcritical, just below or well below the margin of black hole formation, and we again found power-law tails, but not QN ringing. For what can be considered "generic" data (see Paper I), we found that QN ringing disappeared abruptly at the margin of collapse, while the appearance of power-law tails was continuous and unremarkable across the transition from subcritical to supercritical models. This last observation in itself is a very strong corroboration of the simple picture of tail formation set out above. Further evidence can be found in the dependence of the tail amplitude on the amplitude of the initial data, as shown in Fig. 14. The Bondi mass of the spacetime scales as the square of the amplitude of the initial data and we find that the tail amplitude scales as the cube. This suggests that the tails are scattered off the spacetime curvature only once, picking up a single factor of mass.

In a second extension we considered non-spherically symmetric test fields on the dynamical backgrounds generated by collapsing scalar fields. We found that the exponent of the

tails varies with multipole index roughly as for fixed backgrounds. Furthermore we used the fact that QN ringing is less damped in the higher modes to make precise measurements of QN frequencies. For models in which the mass of the background was reasonably constant we found excellent agreement with the predictions on a fixed Schwarzschild background. For models with significant mass loss we found a shift in QN frequency corresponding to the changing mass of the spacetime.

In summary, we found that the predictions for power-law tails of perturbations of Schwarzschild spacetime [3] hold to reasonable approximation, even quantitatively, in a variety of situations to which the predictions might seem initially not to apply.

In the interest of brevity and timeliness, the results reported here do not exhaust the interesting questions that might be asked. It will be particularly interesting to explore in more detail the behavior of power-law tails and QN ringing on the critical boundary between collapsing and noncollapsing initial data. It should be said here that our code is probably capable only of much coarser accuracy than that of Choptuik [11], and will have to be modified for this purpose. On the other hand, our code was adequate for verifying, for our two families of initial data, one of Choptuik's crucial results: that for marginal black hole formation the mass of the hole depends in a universal way on the parameter of the family (in our case the amplitude). See Fig. 15.

We wish to thank Jeffrey Winicour and Roberto Gómez for discussions and for making available their results. This work was supported in part by grant NSF PHY92-07225 and by research funds of the University of Utah. J.P. acknowledges hospitality and support from the Institute for Theoretical Physics at UCSB and the National Science Foundation grant PHY89-04035.

REFERENCES

[1] R. Gómez and J. Winicour, J. Math. Phys. **33**, 1445 (1992).

[2] A. Abrahams, D. Bernstein, D. Hobill, E. Seidel, and L. Smarr, Phys. Rev. D **45**, 3544 (1992); R. F. Stark and T. Piran, Phys. Rev. Lett. **55**, 891 (1985); L. Smarr in *Sources of Gravitational Radiation*, ed. L. Smarr (Cambridge University Press, Cambridge, England).

[3] R. H. Price, Phys. Rev. D **5**, 2419 (1972).

[4] E. Leaver, Phys. Rev. D **34**, 384 (1986).

[5] D. Christodoulou, Comm. Math. Phys. **105**, 337 (1986).

[6] D. S. Goldwirth and T. Piran, Phys. Rev. D **36**, 3575 (1987).

[7] E. Seidel and W-M. Suen, Phys. Rev. Lett. **69**, 1845 (1992).

[8] M. W. Choptuik, D. S. Goldwirth, and T. Piran, Class. Quant. Grav. **9**, 721 (1992).

[9] H. A. Buchdahl, Phys. Rev. **115**, 1325 (1959).

[10] E. Leaver, Ph. D. Thesis, University of Utah (1985), unpublished.

[11] M. W. Choptuik, Phys. Rev. Lett. **70**, 9 (1993).

FIGURES

Fig. 1: The conformal diagram of the spherical collapse spacetime for a final hole mass M_f. Shown is our null grid in relation to the future event horizon $\mathcal{H}_+$, future null infinity $scrit_+$, future timelike infinity i_+, and spacelike infinity i_0. Null grid lines pointing to the top left are lines of constant v; those pointing to the top right are lines of constant u or t_B. Null data are set on the bottom right side of the grid at $u = u_0$. The curved lines from left to right are a) $r = const. < 2M_f$, b) $r = 2M_f$ and c) $r = const. > 2M_f$.

Fig. 2: Our null grid in coordinates $t(u, r)$ and r. The $u = const.$ ($t_B = const.$) grid lines approach the event horizon in a finite interval of u which is an infinite interval of t_B.

Fig. 3: The convergence of $\phi(r = 10, t_B)$ with decreasing grid size. On the vertical axis is the log of the l_2-norm of the error (compared to a very-small-grid numerical solution); on the horizontal axis is the norm of the relative grid size. Data on $u = u_0$ for this solution is a Gaussian $\phi(r)$ with center at 1.0, width 0.1 and amplitude 0.06. The curves correspond to the following sections: $a) 0 < t_B < 10,\ b) 10 < t_B < 20,\ c) 20 < t_B < 30\ d) 30 < t_B < 40\ e) 40 < t_B < 50$. The slope of a is 1.34 ± 0.07 and of d is 1.72 ± 0.04.

Fig. 4: The convergence of $\phi(r, t_B = 50)$ with decreasing grid size. The axes and the initial data are the same as for Fig. 3. From top to bottom are $0 < r < 10$, $10 < r < 20$, $20 < r < 30$, $30 < r < 40$ and $40 < r < 50$. The slope of the top graph is 1.21 ± 0.04 and the slope of the bottom graph is 1.70 ± 0.04.

Fig. 5: Part of a plot of $\phi(r = 10)$ versus t_B, in a region where ϕ is dominated by QN ringing. From bottom to top are shown runs with initial radial grid sizes 1/20, 1/40, 1/80, 1/160 and 1/320. Initial data is the same as in Fig. 3, which corresponds to the formation of a black hole with negligible radiation of mass.

Fig. 6: Results of the same runs as in Fig. 5, but here in a region where ϕ is dominated by the power-law tail. Note that the higher the precision, the smaller the value of t_B where the run stops due to an overflow, here at 53 and 57. From bottom to top the curves correspond to initial radial grid sizes of 1/20, 1/320, 1/160, 1/80, 1/40.

Fig. 7: Log-log plots of $\phi(r = 10, t_B)$ for Gaussian data with different amplitudes. Each plot starts after the last change of sign of ϕ. The amplitudes of the initial Gaussian are a) 0.06, b) 0.034 (marginally collapsing), c) 0.033 (marginally noncollapsing), d) 0.01. The power law nature of all curves is clearly visible; the exponents are a) -2.74, b) -2.63, c) -2.63, d) -2.68, compared to a linearized theory prediction of -3. Only the two collapsing cases, show QN ringing.

Fig. 8: A closeup on $\phi(r = 10, t_B)$ in the region of QN ringing for initial Gaussian data. Solid line: Amplitude 0.034, which collapses marginally, showing QN ringing (the small feature around $t \approx 5$). Dotted line: Amplitude 0.033, which marginally does not collapse. Note the complete absence of QN ringing.

Fig. 9: A closeup of $\phi(r = 10, t_B)$ in the region of QN ringing, for static-static data a) Amplitude 0.50, which collapses, and here shows QN ringing. b) Amplitude 0.35, showing only faint QN ringing. c) Amplitude 0.29, which marginally collapses. d) Amplitude 0.28 which marginally does not collapse. There is no qualitative difference between c) and d), in contrast to the case of Gaussian data depicted in Fig. 8.

Fig. 10: Log-log plots of $\phi(r = 10, t_B)$ for static-static data with different initial amplitudes ϕ_0. Each plot starts after the last change of sign of ϕ. The amplitudes are *a*) 0.5, *b*) 0.29 (marginally collapsing), *c*) 0.28 (marginally noncollapsing), *d*) 0.01. The power law nature of all curves is clearly visible; the exponents are a) -2.08, b) -1.98, c) -1.95, d) -1.86, compared to a linearized theory prediction of -2. The power laws are a) -2.08, b) -1.98, c) -1.95, d) -1.86, compared to a linearized theory prediction of -2. Only curve *a* shows clear QN ringing.

Fig. 11: Test fields $\varphi_l^m(r = 10, t_B)$ on a Gaussian background, amplitude 0.06. The three graphs are $l = 0$, $l = 1$, $l = 2$ (in order of increasing frequency).

Fig. 12: Log-log plots of test fields $\varphi_l^m(r = 10, t_B)$ for different multipole indices l on one background spacetime. The background is evolved from Gaussian initial data for ϕ with amplitude 0.02 (noncollapsing). The initial data for the test field is in each case a Gaussian (the test field amplitude, 1.0, has no significance). From top to bottom the curves correspond to $l = 0, 1, 2, 3$. The best fit for the power law exponents are -2.77, -3.95, -5.94, -8.34, compared to predictions of -3, -5, -7 and -9.

Fig. 13: Log-log plots of test fields $\varphi_l^m(r = 10, t_B)$ for different multipole indices l on one background spacetime. The background is evolved from static-static data for ϕ with amplitude 0.1 (noncollapsing). The initial data for the test field is in each case a Gaussian (the test field amplitude, 1.0, has no significance). From top to bottom $l = 0$, then $l = 1$, $l = 2$ and $l = 3$. The best fit for the power laws exponents are -2.70, -3.66, -5.52, -7.26, compared to predictions of -3, -5, -7 and -9.

Fig. 14: Log-log plots of the initial Bondi mass and the amplitude of the t^{-3} power-law tail $\phi(r = 10, t_B)$, both versus the amplitude of initial data. The upper graph of each pair (full dots) represents Gaussian data, the other (empty dots) static-static data The region of dense data points marks the collapse-noncollapse transition on each graph. Both the initial Bondi mass and the amplitude of the tail scale rather precisely as powers of the initial data amplitude for noncollapsing data. The powers are, for the mass 1.99 (Gaussian) and 1.97 (static-static), and for the tail 3.22 (Gaussian) and 3.01 (static-static).

Fig. 15: Mass of black hole formed versus difference between the amplitude of the initial data and the critical amplitude. On the vertical axis, ln(mass). On the horizontal axis $\ln[(p - p_*)/p_*]$, where p is ϕ_0 or A and p_* its critical value. Empty squares denote static-static data, full squares denote Gaussian data. The fact that the static-static data points are further to the left means that they were measured closer to criticality. This was necessary because the universal power-law behaviour of the mass develops only closer to criticality for static-static than for Gaussian data. The deviation from this behaviour is clear in the plot for the empty squares for $(\phi_0 - \phi_{0*})/\phi_{0*} > e^{-6}$. For smaller values the empty squares fall approximately on a straight line. The sets were shifted vertically (but not horizontally as was done in Ref. [11]) with respect to each other in order to place them on one line. This corresponds to an overall constant multiplicative factor in the black hole mass which is not universal but depends upon the family of initial data (Gaussian or static-static). We assumed $A_* = 0.03280$ and $\phi_{0*} = 0.2860$. Formally, the best fit to the slope (power-law) for Gaussian data alone is 0.39, for static-static data alone 0.31, and combining both sets 0.35. A full analysis of the uncertainties in these slopes has not been carried out, but we assume that within numerical accuracy the slopes agree with each other and with the slope 0.37 found by Choptuik [11].

Figure 1

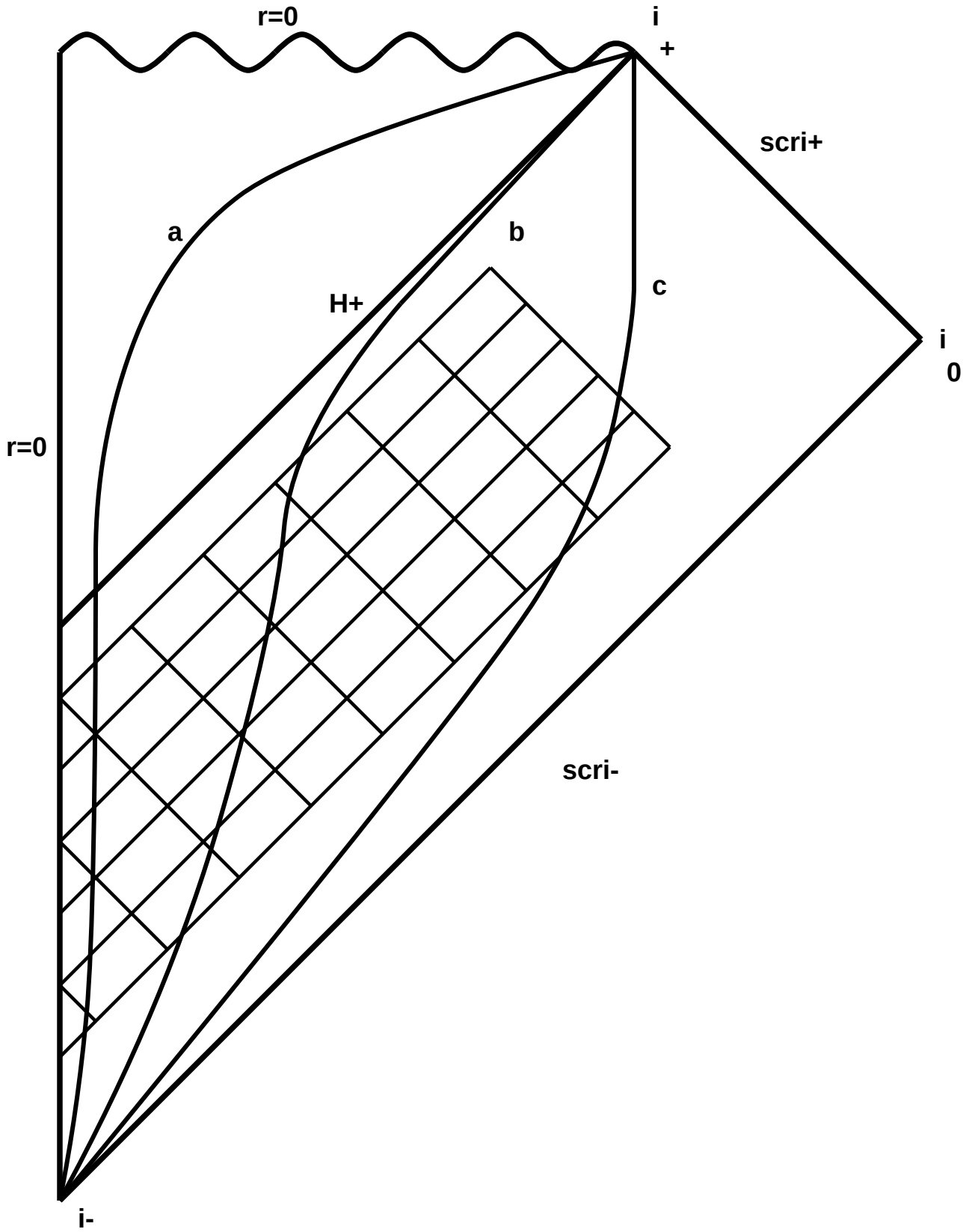

Figure 2

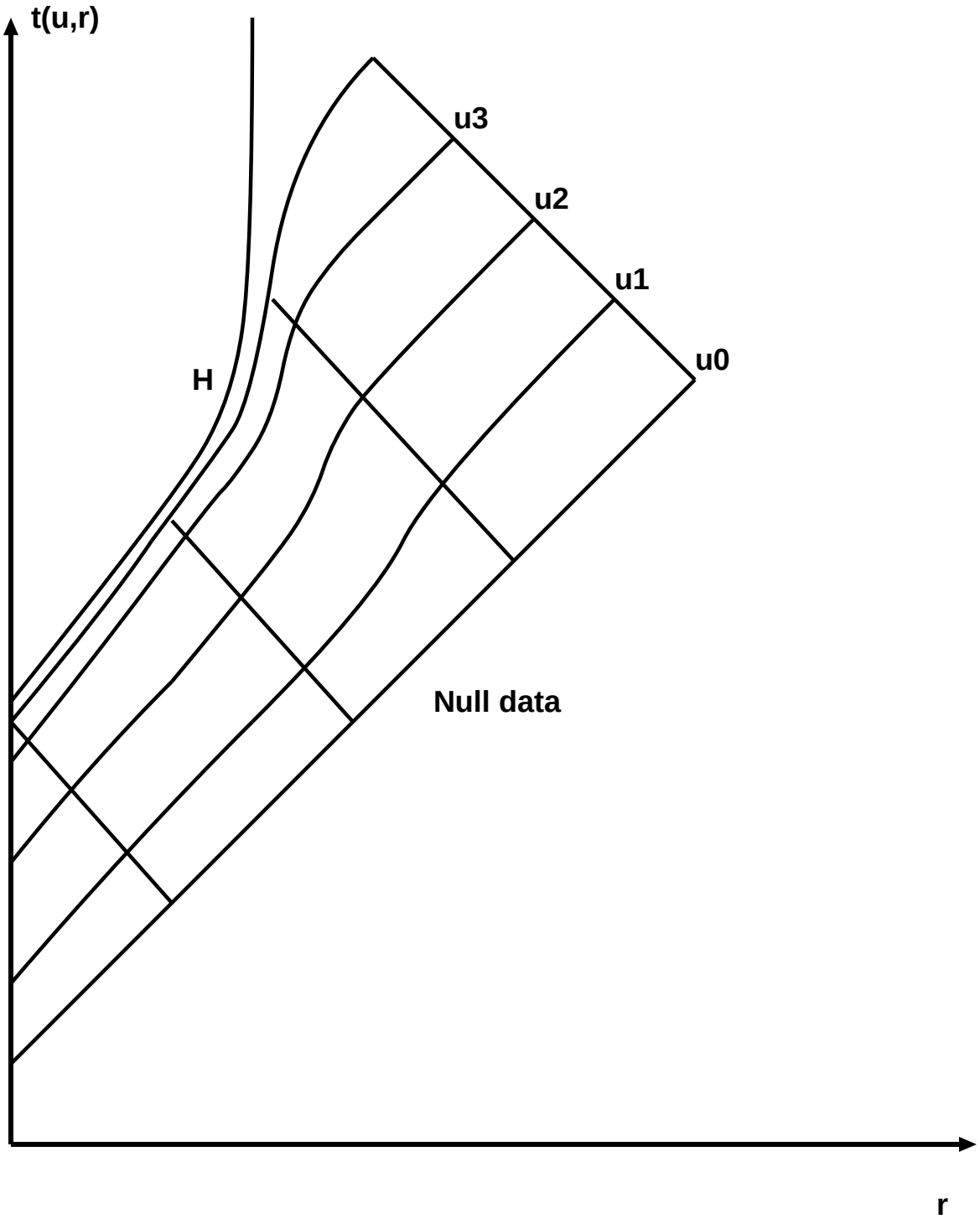

Figure 3

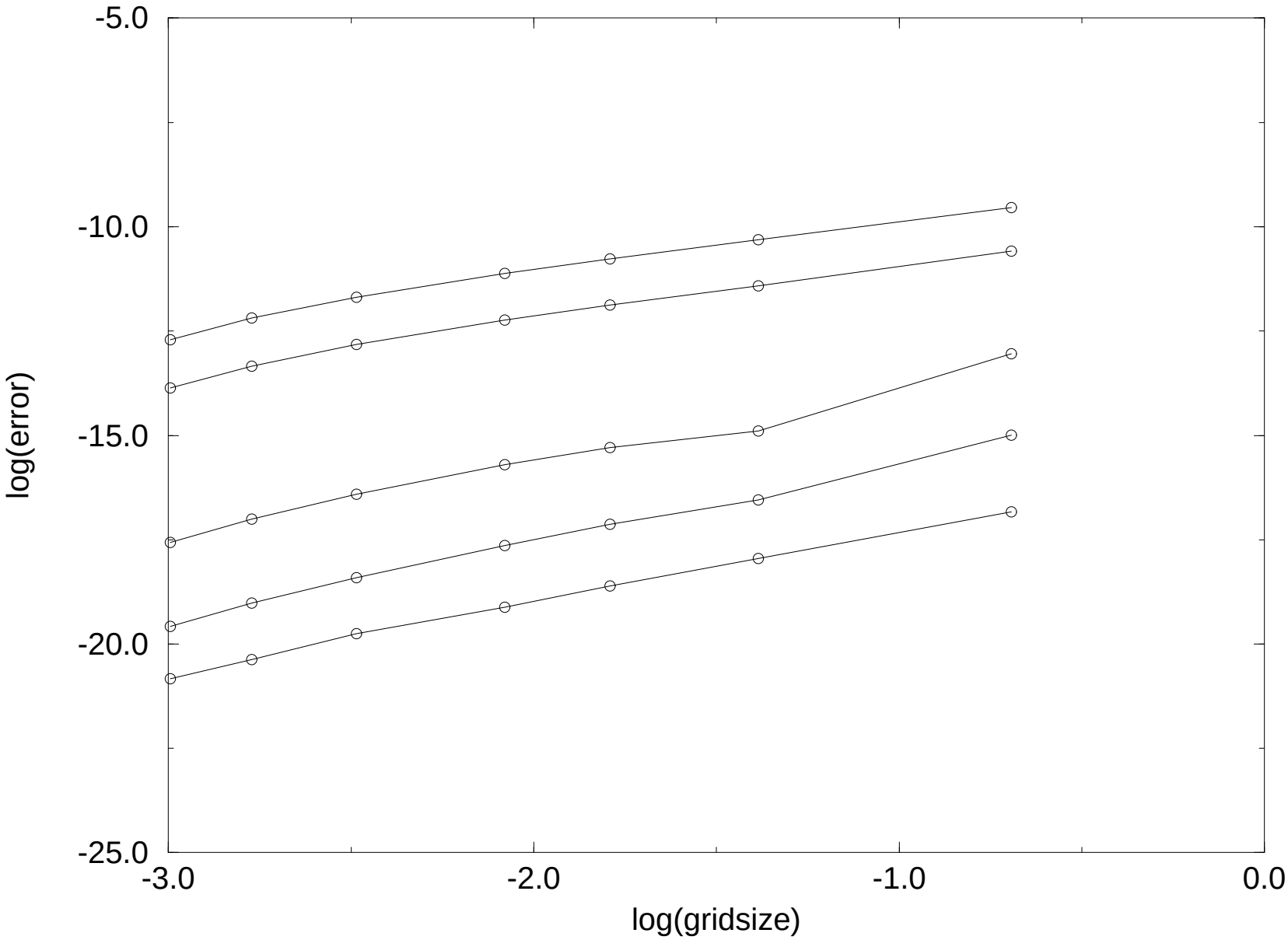

Figure 4

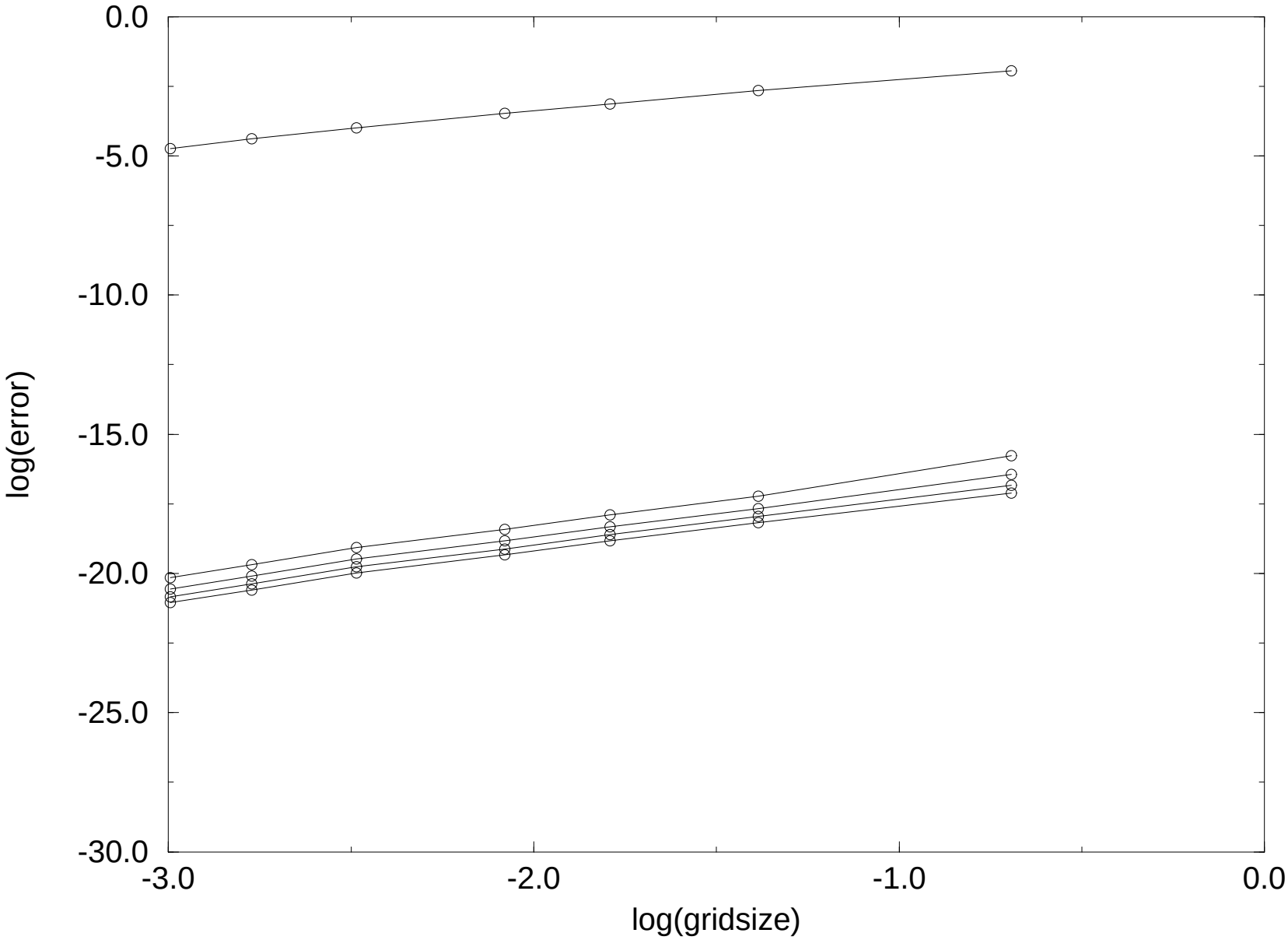

Figure 5

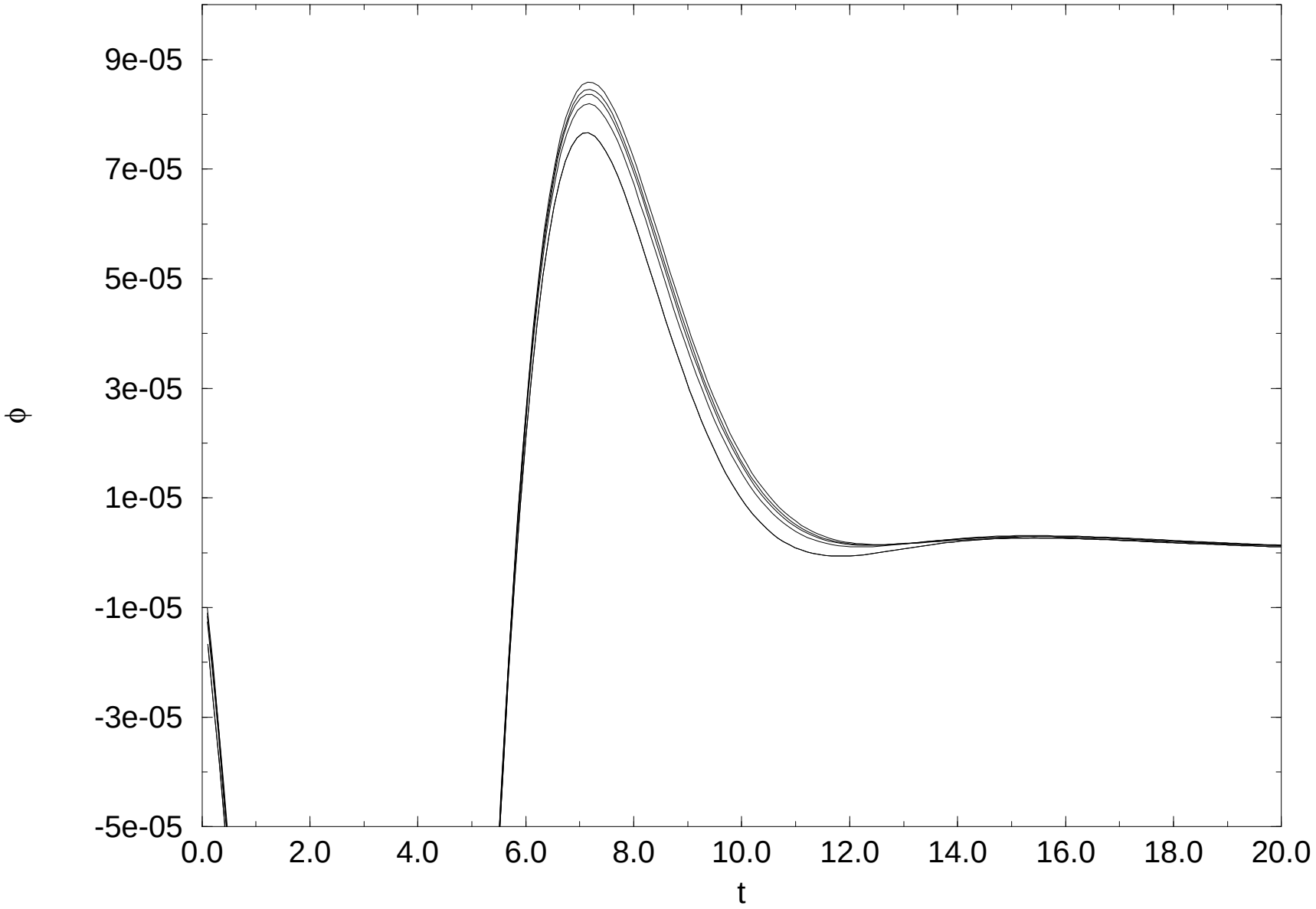
9e-05
7e-05
5e-05
3e-05
1e-05
-1e-05
-3e-05
-5e-05
ϕ
0.0
2.0
4.0
6.0
8.0
10.0
12.0
14.0
16.0
18.0
20.0
t

Figure 6

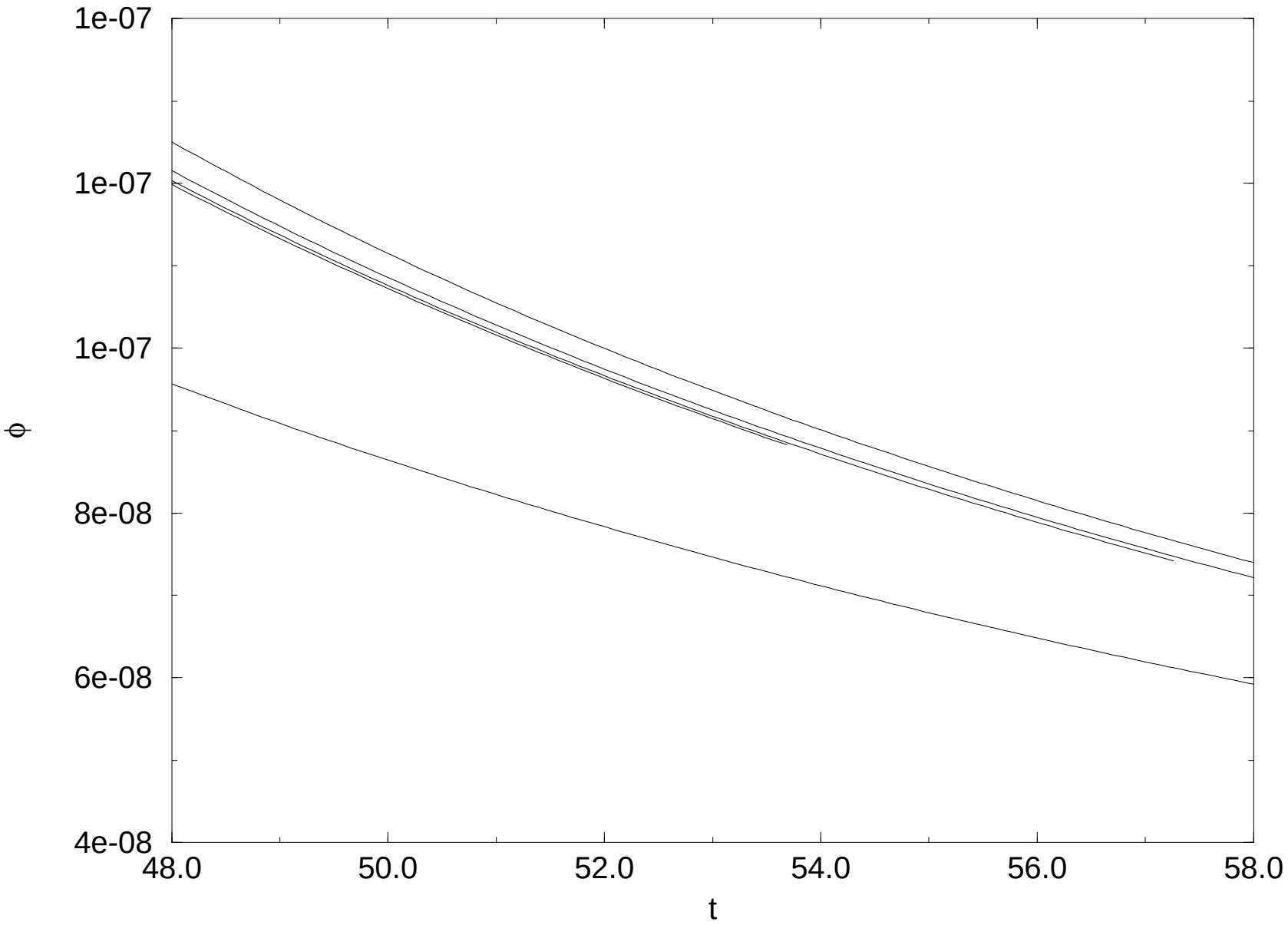

Figure 7

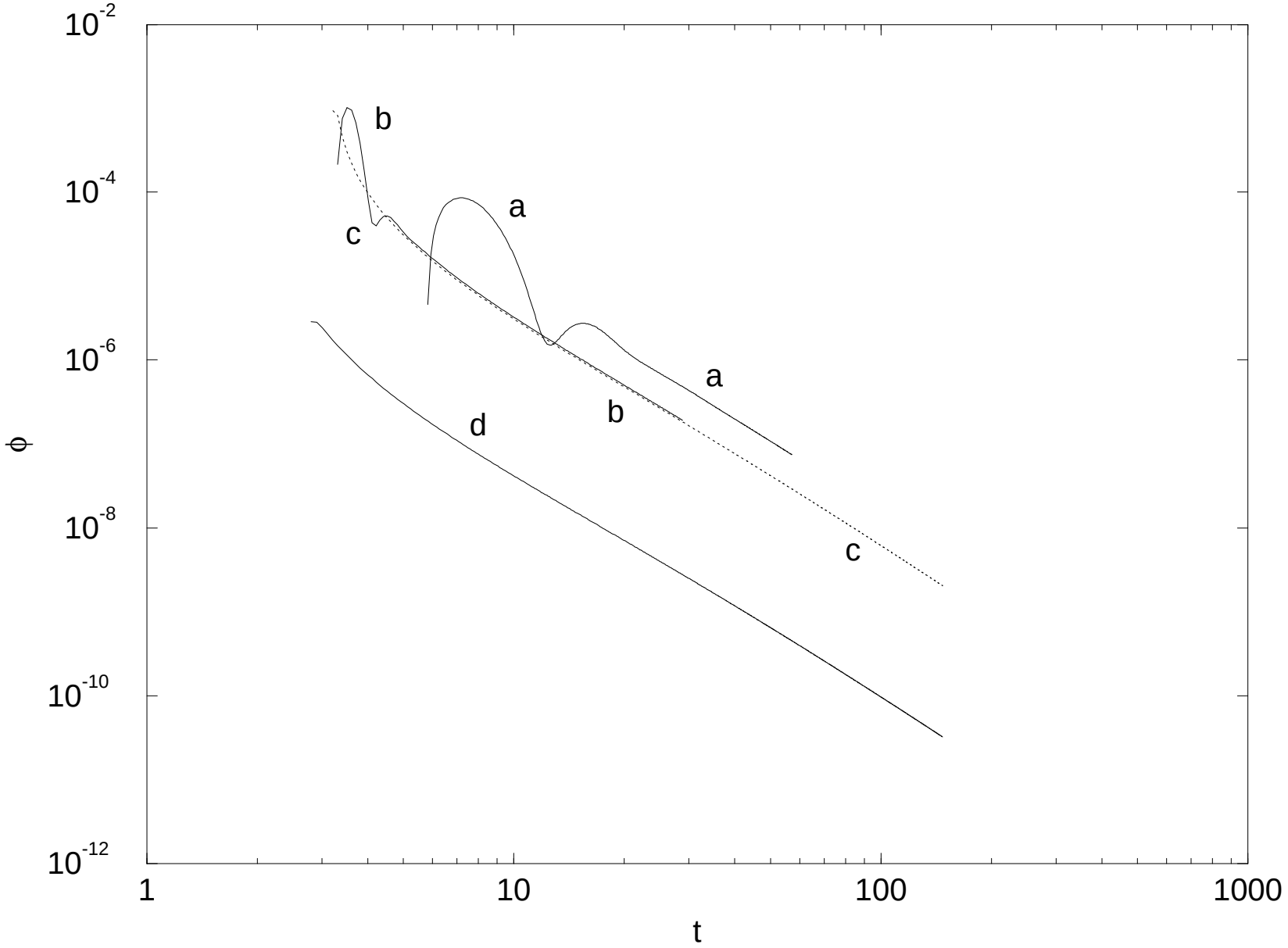

Figure 8

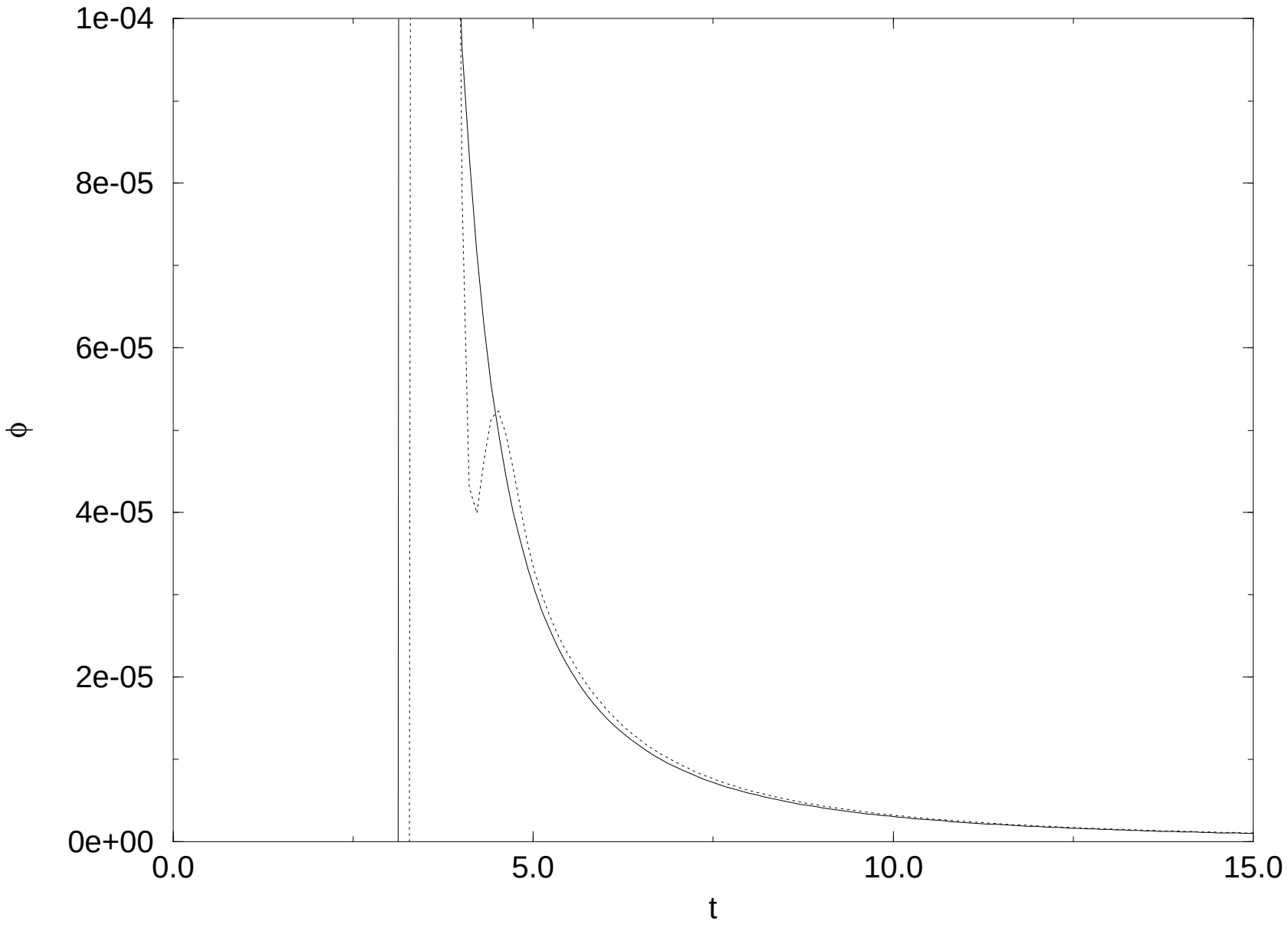

Figure 9

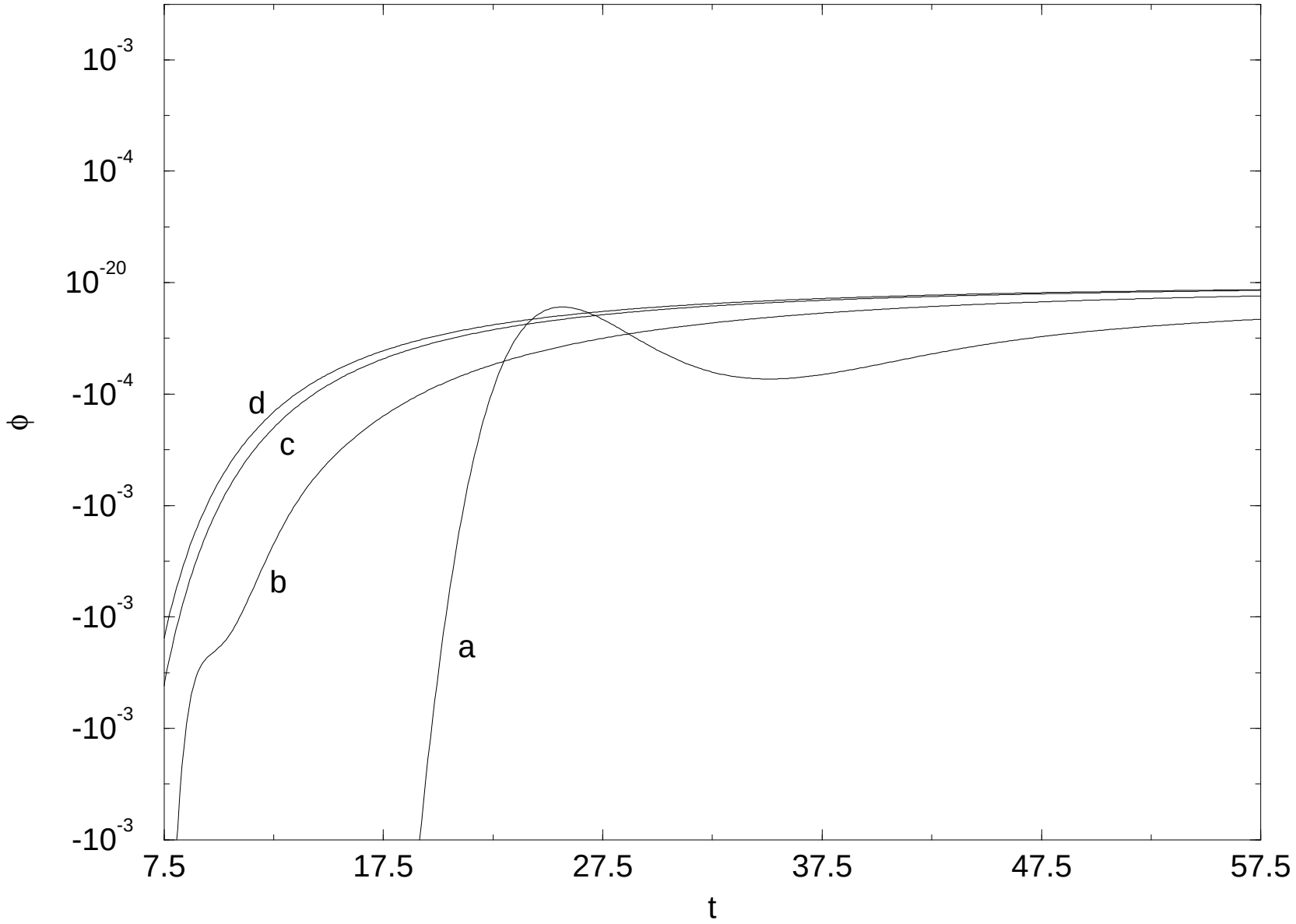

Figure 10

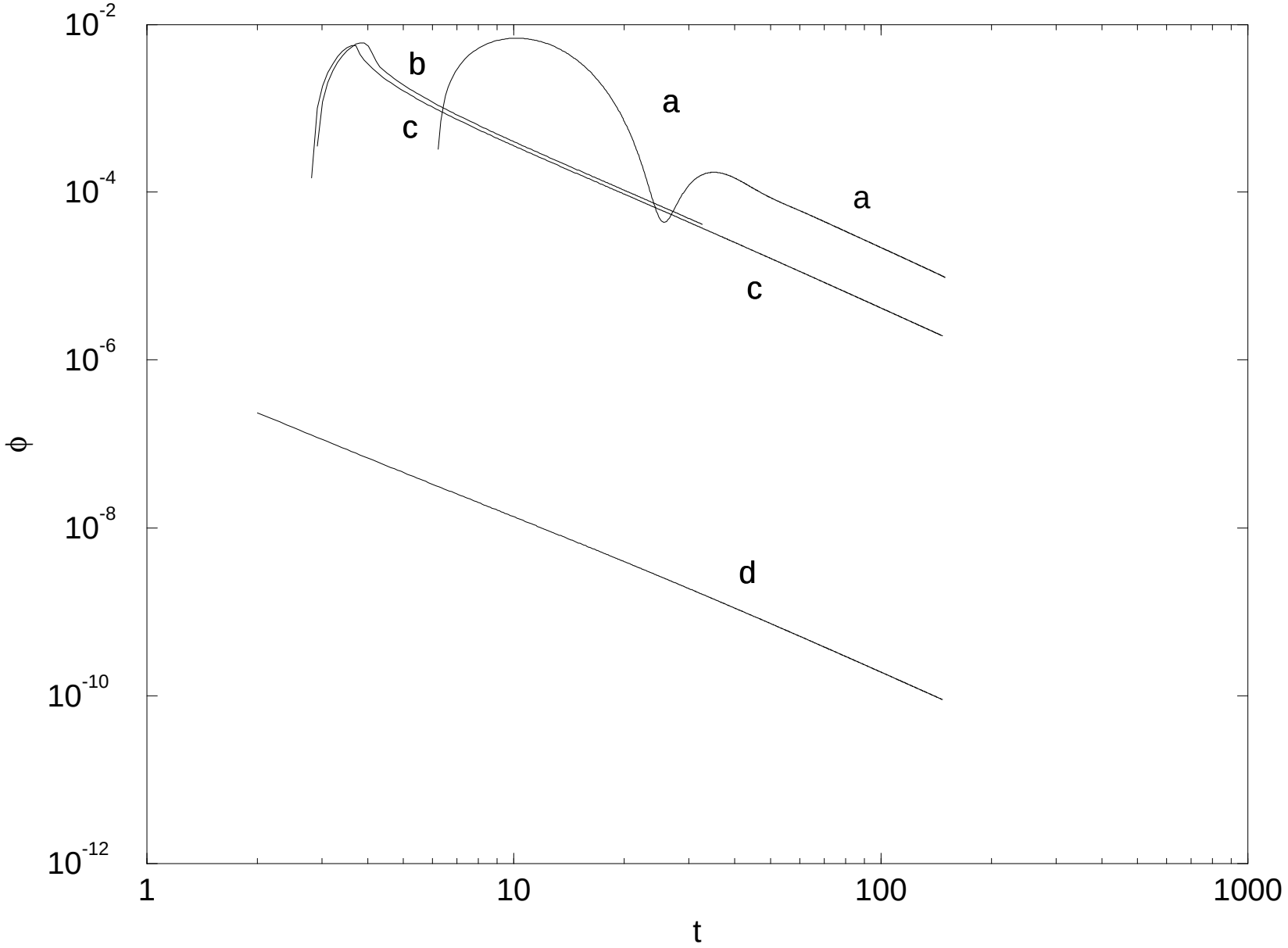

Figure 11

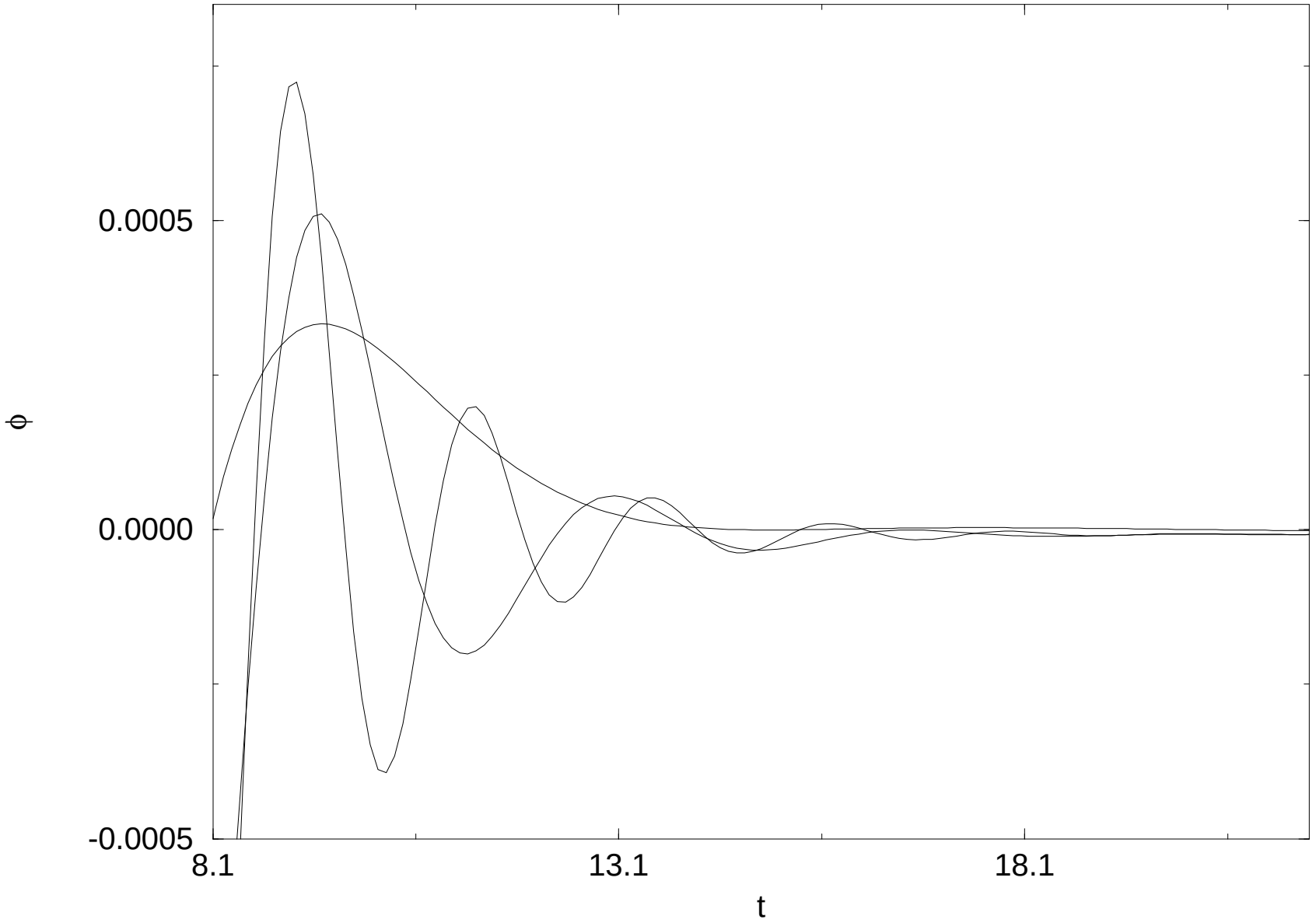

Figure 12

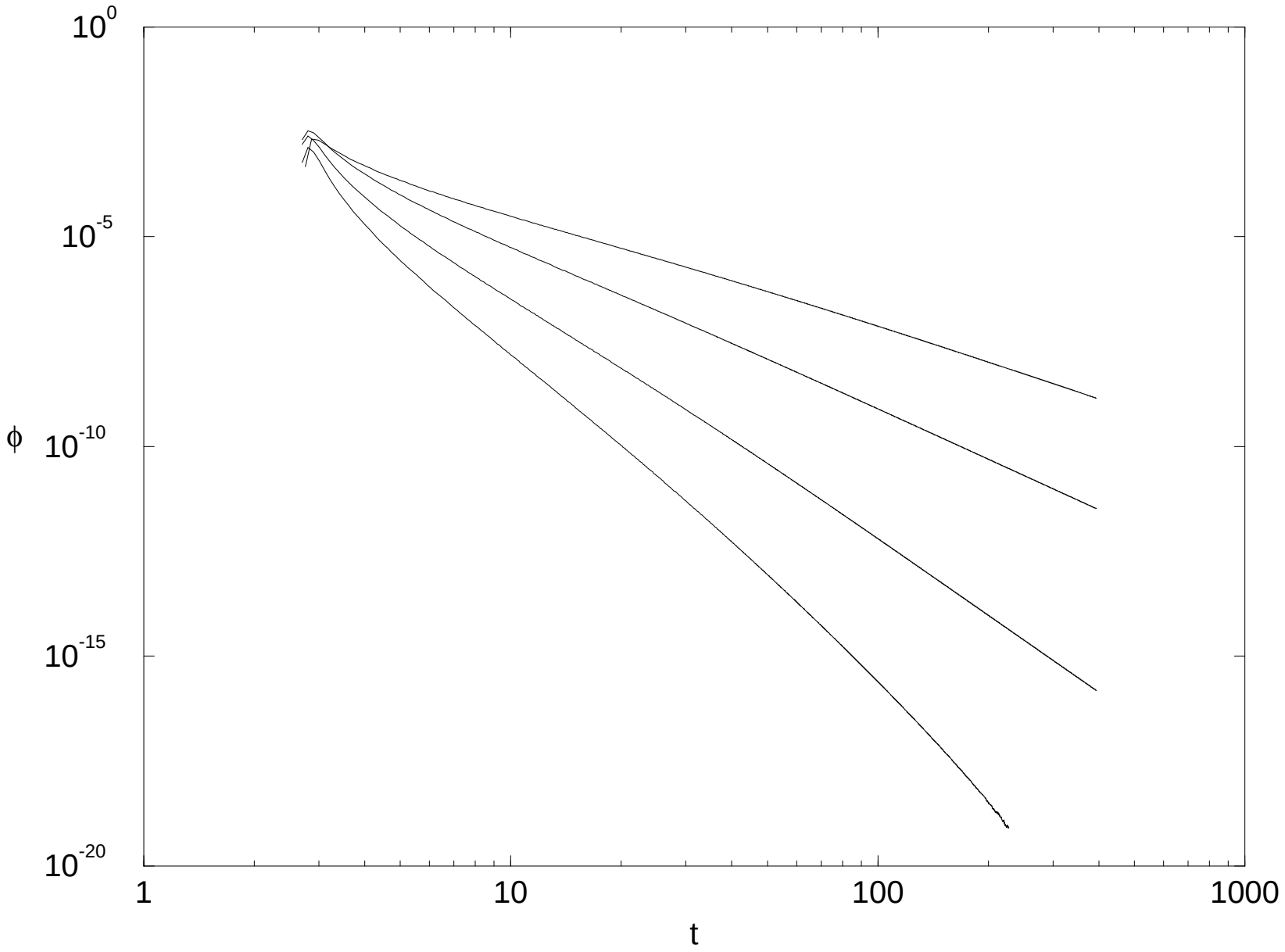

Figure 13

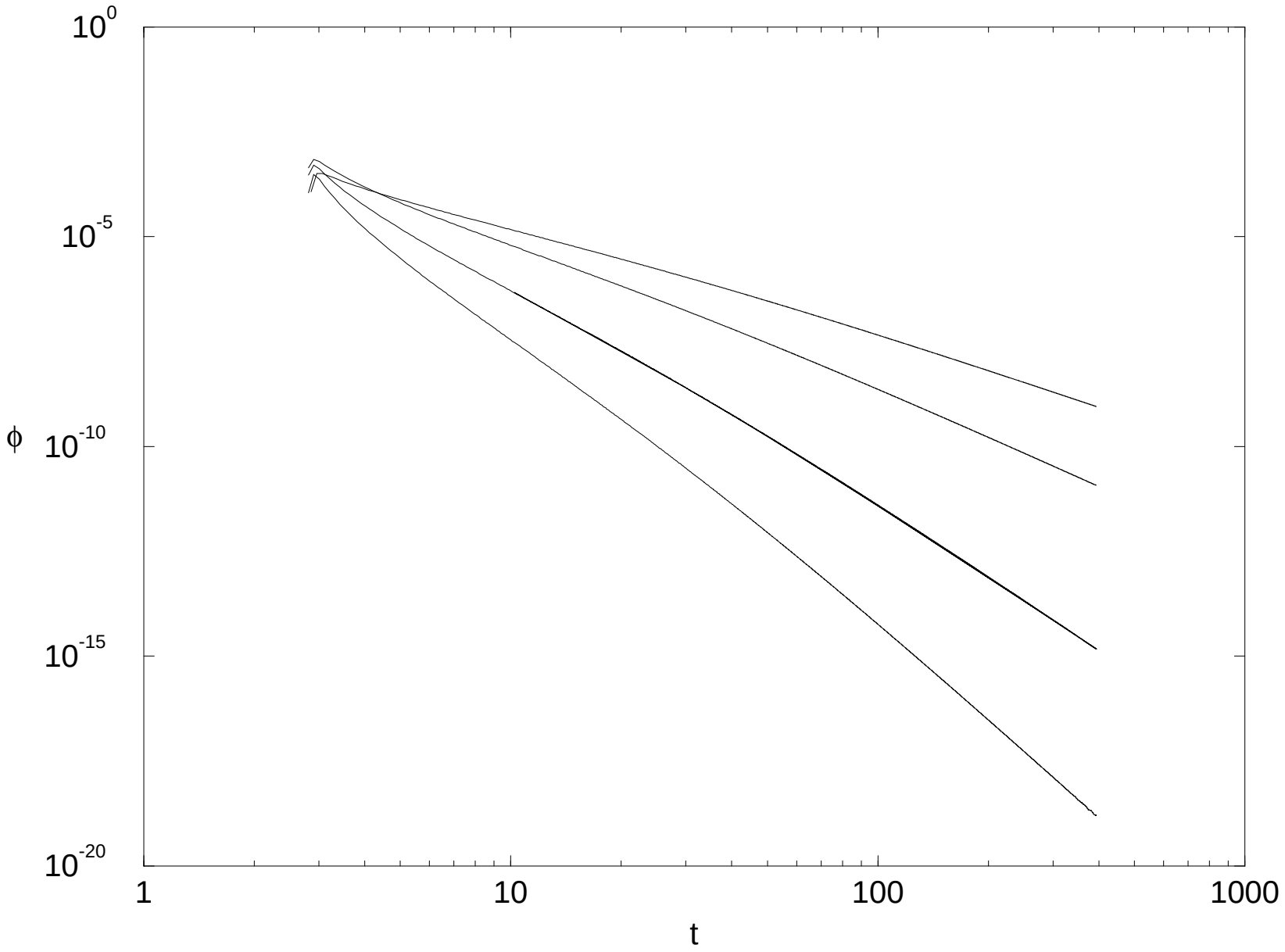

Figure 14

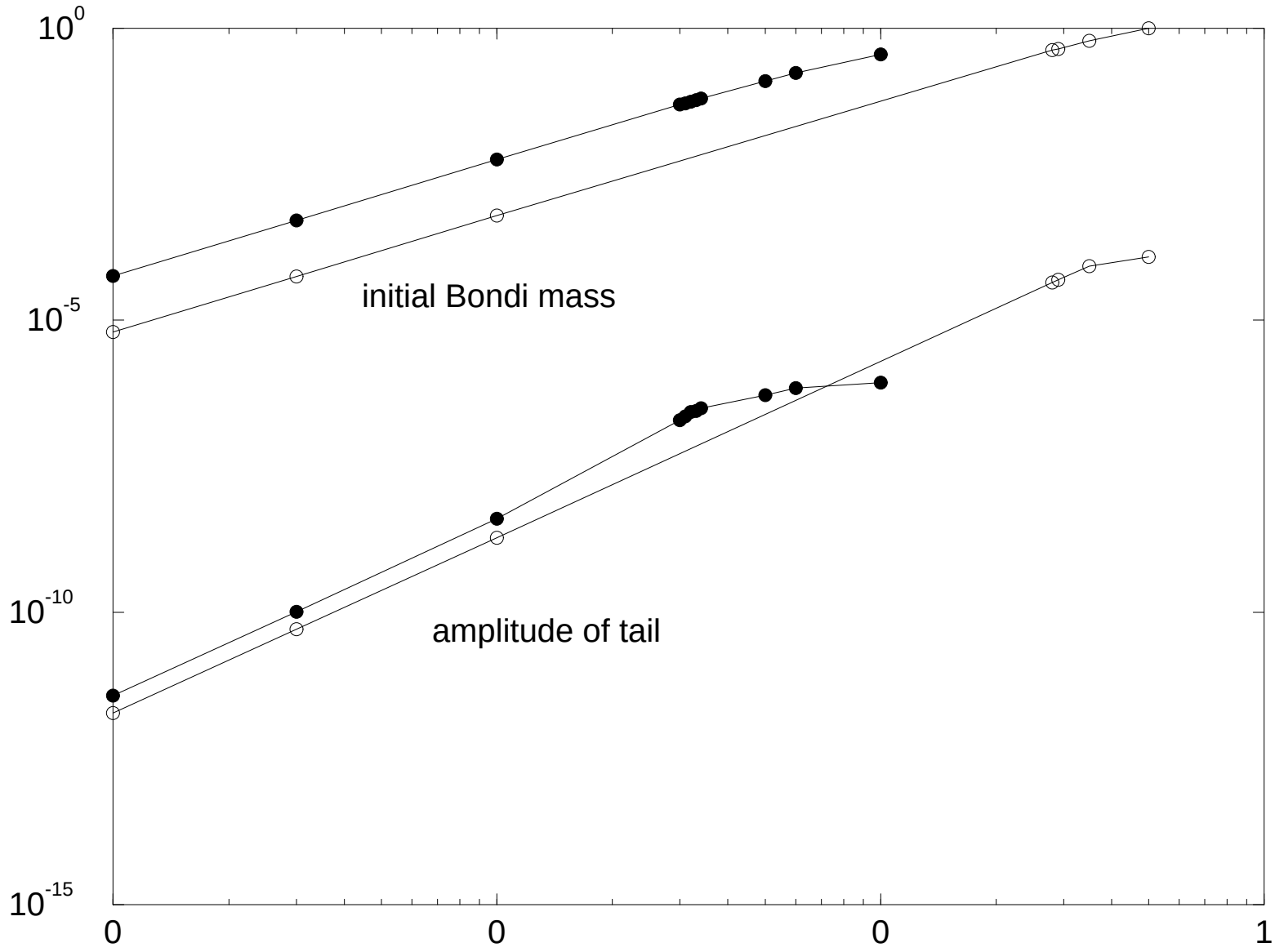

Figure 15